The International Journal of Advanced Manufacturing Technology (2018) 99:623–633
https://doi.org/10.1007/s00170-018-2519-3

ORIGINAL ARTICLE

Weld defect identification in friction stir welding through optimized wavelet transformation of signals and validation through X-ray micro-CT scan

Rohan Basu Roy[1] · Alekhya Ghosh[1] · Soham Bhattacharyya[1] · Raju P. Mahto[2] · Kanchan Kumari[2] · Surjya K. Pal[2] · Srikanta Pal[3]

Received: 12 October 2017 / Accepted: 26 July 2018 / Published online: 8 August 2018

Abstract
For control of real-time Internet of Things (IoT)-based remote welding process, continuous detection of defects occurring in the weld sample is of utmost importance so that welding parameters can be changed accordingly to avoid further occurrence of such defects. Time-frequency domain signal processing method, such as discrete wavelet transform (DWT), can be applied for detection of such defects. DWT continuously decomposes a signal into detailed and approximate coefficients through its associated filter banks and provides a time-frequency domain representation of a signal. Different levels of decomposition capture different frequency components, and hence, there is a need for optimization of the level of decomposition of force and power signals recorded during joining of two aluminum sheets by friction stir welding (FSW), for correct identification and localization of defects occurring in the process. Internal defects in the weld samples are further verified by CT scan images. Statistical tools have been used to study the variations in the DWT coefficients due to both internal and surface defects. An attempt has been made to compare between force and power signals as to which gives better defect detection.

Keywords Discrete wavelet transform · Optimization · Force and power signals · Friction stir welding · Internal and surface defects · Micro-CT scan

1 Introduction

FSW is a new solid state joining process where two metals (same or different) are joined by using a rotating tool. It was invented and experimentally proven by The Welding Institute, UK in 1991 [1]. FSW finds a wide range of applications such as in automobile, railway industries, fabrication of rolling stocks, underground carriages, and goods wagons. In construction industries, aluminum bridges and pipeline constructions are made by this process. Aerospace industries also use FSW to fabricate wings, aviation of fuel tanks, cryogenic fuel tanks for space vehicles, etc. In electrical industries, FSW is used to produce bus bar, electrical motor housing, etc. The FSW tool contains shoulder, and a protruded part which is called a pin. As a rotating FSW tool plunges into the weld zone, frictional heat is generated and the pin provides stirring action on the materials [2]. The temperature increases due to the friction and the relative motion between the tool and the materials. It increases up to a value 0.5–0.6 times the melting point of the metal with lower value of melting point in case of welding of the dissimilar materials. At this temperature, the materials get transformed into plastic stage and are joined by stirring action and axial pressure of the rotating tool, similar to mixing of clay [3]. The process parameters are: tool rotating speed (ω), welding speed (v), tilt angle (α), plunge depth (δ), and tool geometry. Often, various types of surface as well as internal defects occurred in the weld region at improper values of process parameters, such as increased values of ω at the α value of 0° that leads to several surface and internal defects.

✉ Surjya K. Pal
skpal@mech.iitkgp.ernet.in

[1] Institute of Radio Physics and Electronics, University of Calcutta, Calcutta 700 009, India

[2] Department of Mechanical Engineering, Indian Institute of Technology Kharagpur, Kharagpur 721 302, India

[3] Department of Electronics and Communication Engineering, Birla Institute of Technology Mesra, Mesra 835 215, India

These defects lead to the degradation in the mechanical and metallurgical properties.

This process has several advantages. It is energy efficient as compared to other fusion welding techniques such as arc welding, laser beam welding, electron beam welding etc. It has very low environmental impact. The strength of the joint formed by FSW is comparable to that formed by conventional fusion state welding techniques. Since no extra material is used in this process, the composition of the weld is almost the same as that of the original metals taken. However, there are certain limitations too. An exit hole is left behind while taking out the tool from the work surface, at the end of the process. This leads to some amount of material loss. Inappropriate values of process parameters may lead to weak mixing of the materials known as "kissing bond". The use of backing plate is must as the process requires adequate reaction force from the bottom side for producing sound weld.

In this study, an attempt has been made to study the axial force and power signals of FSW. The magnitude of the force depends on the resistance by the weld materials on the FSW tool. In addition, its values are significantly higher as the tool has greater interaction with the weld materials. Abrupt changes in the force or power indicate change in its interaction between the weld materials so they reflect defects (internal or surface) [4]. Due to improper process parameters and heterogeneity of the materials, welding may be affected. Scanning the welded zone at each moment during the welding process to locate defects is time consuming and also a costly affair. So, it is easier to study the output variables such as force signal or power signal of the job. In this paper, distortion in the power and force signals are used as a measure of defect analysis during the welding process. The signals were recorded using force and power sensors. For time-frequency domain representation of the signals, DWT is deployed to localize the defects.

Till date, researchers have worked on FSW axial force, v, ω, torque, and various other factors to establish their interrelationship and choose the parameters accordingly to produce sound weld. It was observed that the FSW force versus time plot has an initial high value and then drops down to a lower one, there after remaining steady till the end of the welding period [5]. It was shown that tangential force can be measured in order to compute coefficient of friction by using load cell [6]. A relation was established between tangential force and coefficient of friction. A generalized relation between torque (M_Z) as a function of ω, v was established [7]. The authors showed that M_Z decreases exponentially with the ω, whereas v has a linear relationship with M_Z . From the study of welding forces and heat input with varying parameters, it was concluded that ω, v, and tool shoulder diameters are the most significant parameters that affect axial force and heat input [8]. A model capable of predicting tool forces for different welding parameters and regions of tool failures was developed [9]. It helped to identify tool pin designs to process the work-piece more efficiently. It was shown that the force reaches to a maximum value during plunge stage and experiences a fall of 35% during translational stage. A torque-based model for various alloys (7075, 5083, 2024) was developed and their relationship between FSW parameters was studied [10]. A methodology was proposed in which the currents and power transients of the electrical motors (which drives the motions) were monitored to measure the torque and the traverse force [11]. In the method, use of costly dynamometer was avoided and the process was completely independent of changing welding conditions. The best welding conditions are achievable at low welding speed ($\leq$40 mm/min) and high rotational speed ($\geq$ 1000 RPM) in FSW of AA2024-T4 aluminum alloys [12]. It was found that joint fabricated with an axial force of 5 kN exhibits superior tensile properties as compared to several other joints and axial forces significantly influence the formation of defects [13]. For very small α ($\leq$1.5°) or very large α ($\geq$4.5°), main defects are formed for butted 6061 aluminum alloy plates having three equal gaps [14]. Variation of α affects plastic material flow patterns in the stir zone which in turn controls the weld properties. The authors also pointed out that oxide of aluminum is the major cause of formation of defect at the welding region. Welding parameters like v, ω, δ, etc. were optimized to obtain a weld free of internal defects [15]. By controlling the geometric parameters, the number of defects can be lowered [16].

Artificial neural networks (ANN) were used to find correlation between acoustic signals emitted by FSW process and the parameters of it [17]. They used statistical and temporal parameters of the discrete coefficients obtained from the wavelet analysis as the input of the ANN. Discrete wavelet transform (DWT) was used to show band energy of decomposed acoustic emission in signals as a measure to judge defects in weld [18]. Fast Fourier transform (FFT) and DWT were applied on force signals to show the effects of changing parameters in FSW. It was stated [19] that signals that were in the higher frequency range disappeared if the contact between the tool and the job is lost. An attempt was made to monitor FSW process by analyzing the weld surface images and classify good and defective weld using support vector machine [20]. DWT was used to obtain the useful features of the images and classify the defects into good and bad welds.

FSW voltage and current signals from main spindle motor and current signal from feed motor were obtained and regression models were developed to correlate the signal characteristics with ultimate tensile strength (UTS) and yield strength (YS) of joints. It was found that main spindle motor current signal influenced UTS and YS most [21]. Authors developed a model for effective monitoring of the FSW process with recorded signals for better control of outcome of the process.

Table 1 Process parameters of the welding process

Process parameters	Values (sample 1)	Values (sample 2)
ω	500 rpm	2000 rpm
v	40 mm/min	40 mm/min
δ	0.1 mm	0.1 mm
α	0°	0°

In reference [22], researchers applied Fast Fourier transform, DWT, and other signal processing techniques on acoustic emission signal to identify defects in FSW. DWT was applied on force signal data to localize the surface weld defects [23]. In reference [24], researchers proposed a method to determine the best possible basis function for wavelet packet decomposition based on energy to entropy ratio of the decomposed coefficients. This method

Fig. 1 NC-controlled FSW machine

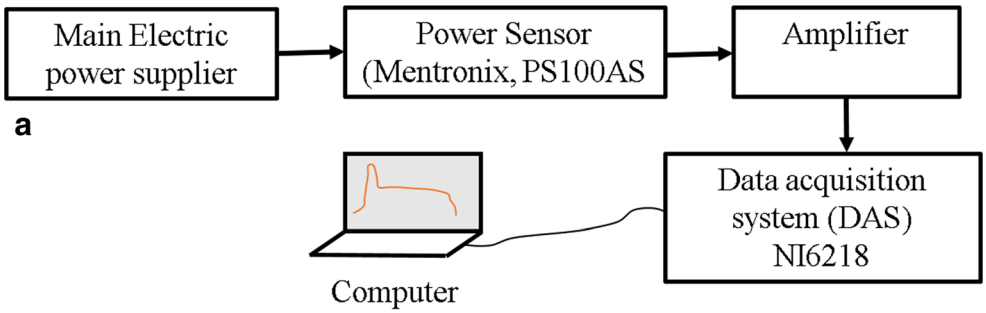

a

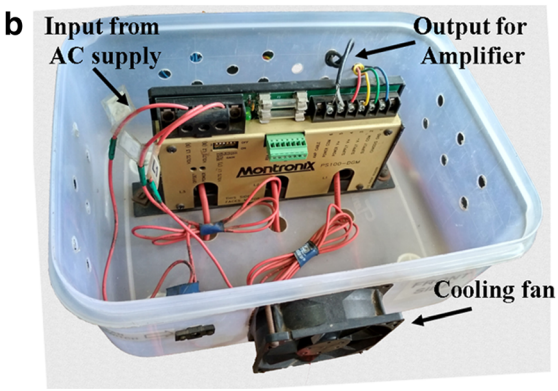

Fig. 2 **a** Schematic diagram for integration of power sensor with machine. **b** Power sensor

was utilized for feature extraction to determine the weld quality. The authors have also shown that prediction of UTS and YS of weld from decomposed wavelet packets can be better performed by a multi-layer feed forward neural network than a network model based on radial basis function. Various real-time image processing techniques have been applied to study the variation of weld quality due to pin failure and pin depth change in FSW [25].

In reference[26], a genetically optimized artificial neural network structure is developed which uses five neural networks to predict UTS, YS, elongation, hardness (weld mat), and hardness (Haz) which are used to predict ω and v. These parameters were used as feedback inputs for the neural networks. Reliable weld quality was prediction models that were built from weld parameters like ω, v, δ, and using techniques like K-nearest neighbor, bee colony optimization to save manufacturing cost [27]. Adaptive neuro fuzzy logic-based models were used for optimization of FSW process parameters to obtain desirable mechanical properties of the weld [28]. Optimum parameter prediction for FSW was done by using genetic algorithm [29] and various experimental design techniques [30, 31] to maximize weld quality. FSW defects were detected using fractal dimensions of signals for plunging, dwelling, and welding stages [32]. Image processing algorithms like image pyramid [33] were used to classify various defects like voids, cracks, grooves, flash, keyhole, etc. occurring in FSW [34]. Defect detection of FSW defects was done using scalogram of continuous wavelet transform (CWT) coefficients of force signal [35], wavelet packet decomposition, and Hilbert–Huang transform [36]. Volumetric defect analysis in FSW based on 3D reconstructed weld surface images was performed for detection of defect volume [37]. Optimization of FSW parameters was carried out to obtain desired UTS, compressive strength, welding angle, weld bead thickness, etc. using hybrid fuzzy Taguchi based method [38]. Reflection of ultrasonic waves incident with multiple angles was used for FSW defect identification [39].

There have been several researches on FSW parameter optimization, surface defect detection, and classification using various signal and image processing techniques. But for

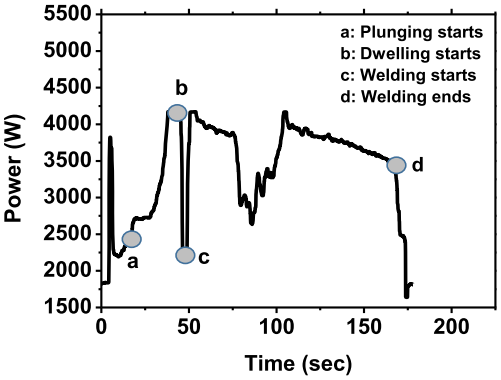

Fig. 4 Plot of variation of power with time of sample 2

Industrial Internet of Things (IIoT)-based applications, it is necessary to reduce time complexity. Here, we have used DWT to exactly localize both surface as well as internal defects occurring in FSW. DWT has the time complexity in the order of $O(log_2 n)$, where n is the number of samples in the analyzing signal. This is suitable for IoT-based applications. Previous researches using wavelet transformation for defect detection did not specifically mention the required number of levels of wavelet decomposition for defect detection. If we take into consideration all the possible levels of decomposition, the computational time will increase. Here, we have optimized the number of levels of wavelet decomposition for weld defect localization using a coefficient of error localization (χ_e), a factor defined in Sect. 2.4. This work is focused to study the DWT coefficients of both FSW force and power signals. χ_e had also been used to compare between the two signals as to which gives better defect localization. Voids and defects occurring inside the surface of the weld are validated through CT scan images. Statistical tool, square of mean deviation, which is also termed as square of errors is used to localize the defects. This kind of continuous defect localization technique can be applied for real-time applications in a sense that once a defect is localized, FSW parameter values can be changed accordingly to avoid their further occurrence. This scheme for defect detection can be embedded in an IoT device for online defect monitoring and control in FSW.

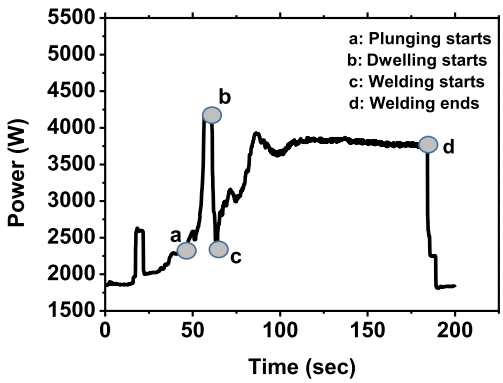

Fig. 3 Plot of variation of power with time for sample 1

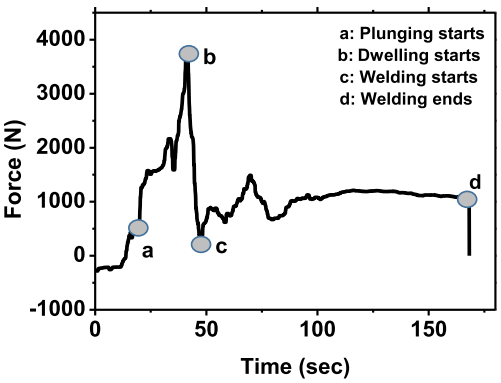

Fig. 5 Plot of variation of force with time for sample 1

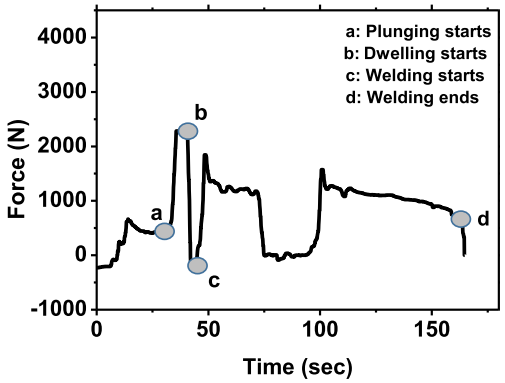

Fig. 6 Plot of variation of force with time for sample 2

2 Experimental details

2.1 Experimental set ups and methodology

FSW was used to produce butt joint between 2.5-mm-thick sheets of commercially pure AA1100. Chemical composition of work material was studied with the help of optical emission spectroscopy (ARL 3460). The length and the width of the rectangular samples were 100 and 45 mm, respectively. The sheets were cleaned properly and placed along 100 mm length in FSW fixture. A FSW tool made up of H13 carbon steel has a cylindrical pin. The height of the pin was 2.1 mm, whereas the diameter of shoulder and pin was 16 and 5 mm, respectively. The experiments were carried out at ω and v of 500 rpm, 2000 rpm, and 40 mm/min, by keeping a constant value of δ and α at 0.1 mm and 0°, respectively (Table 1). All the experiments were carried out at displacement control mode.

FSW experiments were done by a 2.0 ton NC FSW machine manufactured by ETA Technology Pvt. Ltd., India, as shown in Fig. 1. The machine had several sensors integrated to it to measure X-position of the tool, ω, M_Z, X-velocity, X-load, Z-position, etc. A power sensor (Montronix, PS100AC) connected externally measures power consumed during the process. Figure 2 shows schematic diagram of integration power sensor with machine. The machine also has a load cell integrated to it to measure forces along the Z direction. A three phase AC induction motor rotates the tool and drives the main spindle. The machine was connected to a PLC-based control system with PC and LabVIEW software for real-time data acquisition. The data obtained for vertical axial force from the load cell was used for the processing. Further, a laboratory-based high-resolution 3D X-ray micro-CT system with open and close tube X-ray source configurations was used for scanning the weld in order to find internal defects such as voids, kissing bond, etc.

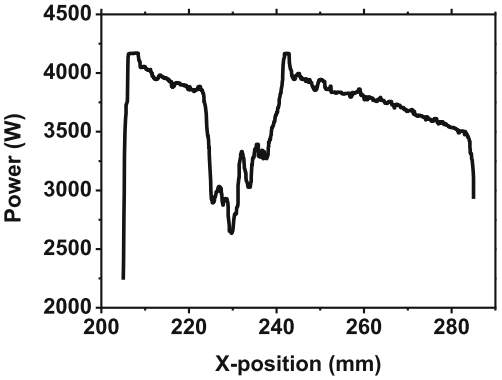

Fig. 8 Plot of power versus X-position of the welding tool in the welding zone for sample 2

2.2 Signal processing

Traditional time domain analysis of signals fails to present a picture of the frequencies (spectral components) present in a signal. Fourier transform (FT) of a signal represents the frequency domain plot. The discrete time Fourier transform (DTFT), discrete Fourier transform (DFT), fast Fourier transform (FFT), discrete cosine transform (DCT), etc. are frequency domain analyses of discrete time signals. But the major drawback of these transformations is that they are effective only for stationary signals. To know exactly what frequencies are present at a particular time, time-frequency domain analysis is useful.

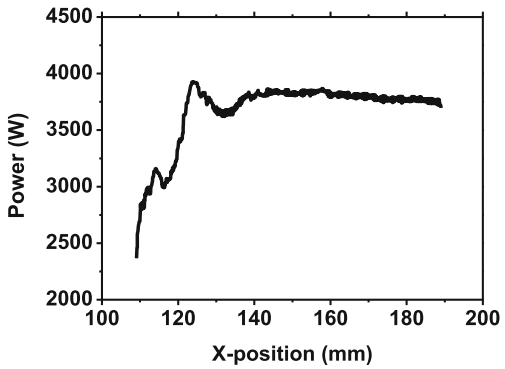

Fig. 7 Plot of power versus X-position of the welding tool in the weld zone for sample 1

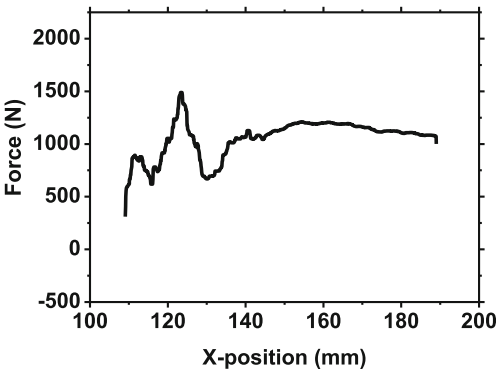

Fig. 9 Plot of force versus X-position of the welding tool in the weld zone for sample 1

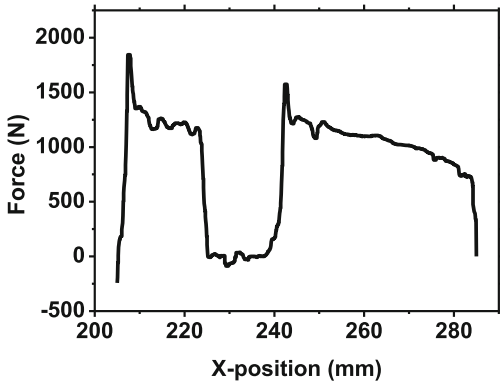

Fig. 10 Plot of force versus x-position of the welding tool in the weld zone for sample 2

The short time Fourier transform (STFT) is a primitive time-frequency domain analysis where a window of finite width is chosen and shifted along the direction of the signal. The window function is multiplied with the signal and the Fourier transform of the effective is taken which gives an idea of within what range a particular frequency is present. But due to the constant width of the window, several problems related to resolution occur.

2.3 Discrete wavelet transform

To solve this ambiguity, DWT method is found to be most suitable. In DWT, a mother wavelet is scaled and translated along the entire duration of the signal to obtain the required child wavelets. This solves the resolution problem occurring in STFT. DWT is used when the input signal is discrete. Wavelet coefficients are given by Eq.1.

$$A = \int_{-\infty}^{\infty} x(t) \frac{1}{\sqrt{2^j}} \Psi\left(\frac{t-k2^j}{2^j}\right) dt \tag{1}$$

where $x(t)$ is the given signal, j is the scale parameter, k is the shift parameter, and $\Psi(t)$ is the chosen mother wavelet.

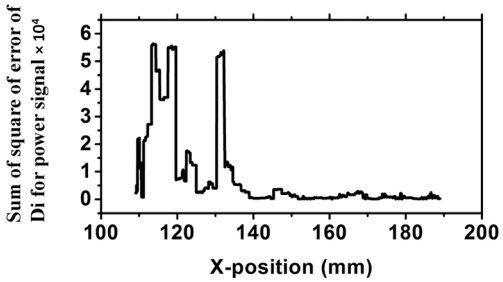

Fig. 11 Sum of square of errors of detailed coefficients (D_i) of power signal up to 5th level of decomposition for sample 1

The computation of DWT is done by passing the signal through high-pass and low-pass filters. The output of high-pass filters after down sampling gives the detailed coefficients (Eq. 2), whereas the same for the low-pass filters, it gives approximate coefficients (Eq. 3).

$$C_D[k] = \sum_N x[n].g[2k-n] \tag{2}$$

$$C_A[k] = \sum_N x[n].h[2k-n] \tag{3}$$

These coefficients are actually values of convolution of input signal and impulse response of the filters. To increase frequency resolution, the output of the low-pass filter is again passed through high- and low-pass filters to obtain detailed and approximate coefficients, respectively. This process is repeated.

Here, in this study, it has been attempted to optimize the level up to which such decomposition of force and power signals are to be carried out for the best detection of defects in FSW. The approximate coefficients signify rough features of the signal, while detailed coefficients capture the distinct features of force signal. By studying these, detailed coefficients for abrupt changes and defects in FSW can be detected.

DWT has varied applications which include data and image compression. Also, it is used in fields of pattern recognition, texture analysis, noise recognition, etc.

Table 2 Comparison of coefficient of error localization of force and power signals at different levels of sum of squares of errors of detailed coefficients

Sum of squares of errors of detailed coefficients up to level D_i	Sample 1		Sample 2	
	χ_f (coefficient of error localization of force signal)	χ_p (coefficient of error localization of power signal)	χ_f (coefficient of error localization of force signal)	χ_p (coefficient of error localization of power signal)
D_2	−0.62	0.06	−0.14	−0.81
D_3	−0.91	−0.41	−0.08	−0.83
D_4	0.38	−0.3	−0.25	−0.32
D_5	0.63	0.73	0.13	0.62
D_6	0.01	0.13	−0.29	0.03

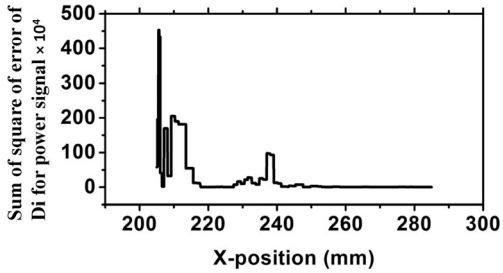

Fig. 12 Sum of square of error of detailed coefficients (D_i) of power up to 5th level of decomposition for sample 2

2.4 Square of errors (statistical parameter)

It is the square of difference of each term from the mean value of the terms. Example: Let a, b, c, … be a set of data with mean value K. Then, $(a-K)*(a-K)$, $(b-K)*(b-K)$, $(c-K)*(c-K)$, … are the square of errors or square of mean deviation terms.

2.5 Experimental procedure for accurate defect detection

I. From the data collected by the force and power sensors during the welding process, the plots of force versus time and power versus time, respectively, were obtained. The plunging and dwelling periods of the process comprise high-frequency components. For defect detection, the plunging and dwelling were subtracted from the plot so that only defects occurring in the welding period can be obtained.

II. From the discrete-time force and power signals of a weld sample, wavelet analysis was done using 'Daubechies' as the mother wavelet to obtain a time-frequency domain representation.

III. The force signal was decomposed at levels 1 and 2, separately. The square of errors at each point of the signals was calculated. Then, the sum of squares of errors of the two signals was calculated and named D2. Similarly, the signal was decomposed at level 3; the sum of squares of errors of the first three levels were calculated and named D3. In the same procedure, D4, D5, and D6 were calculated. The same process was carried out for the power signal as well.

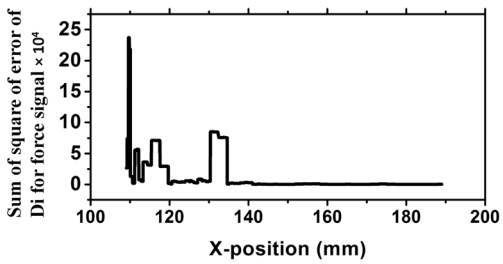

Fig. 13 Sum of square of errors of detailed coefficients (D_i) of force signal up to 5th level of decomposition for sample 1

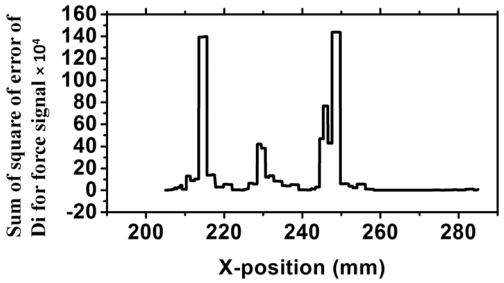

Fig. 14 Sum of square of errors of detailed coefficients (D_i) of force signal up to 5th level of decomposition for sample 2

IV. The sum of square of errors of the weld region was plotted against X-position of the welding tool. Sudden high fluctuations in the square of error plot correspond to sudden changes in the force or power data. So, it can be said that sudden variations in the plot corresponds to defects in the weld.

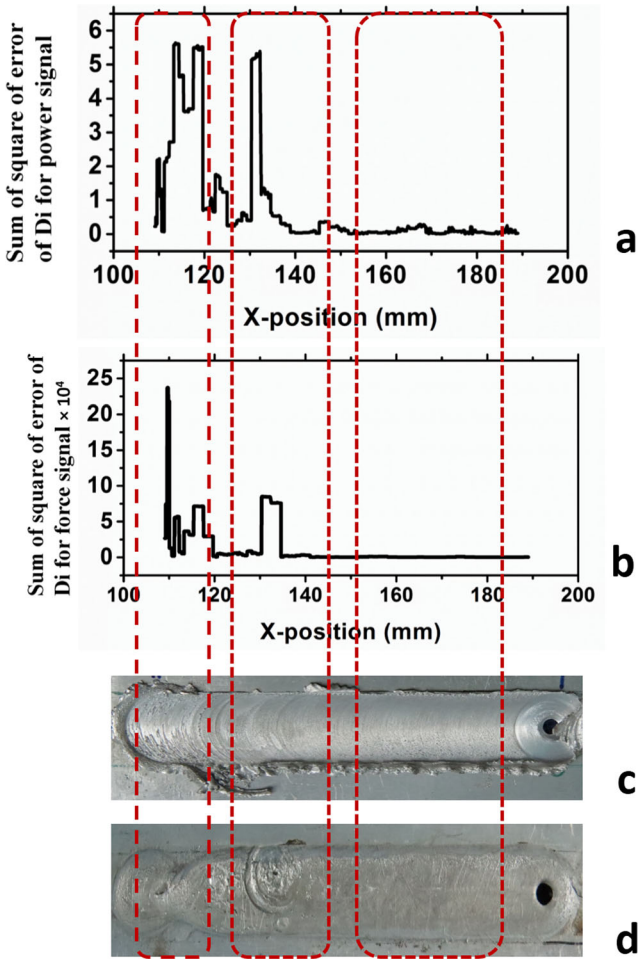

Fig. 15 **a** Plot of sum of square of errors of detailed coefficients (D_i) up to 5th level of decomposition of power signal versus X-position of the tool for sample 1. **b** Plot of sum of square of errors of detailed coefficients (D_i) up to 5th level of decomposition of force signal versus X-position of the tool for sample 1. **c** Front side of the welded sample 1. **d** Back side of the welded sample 1

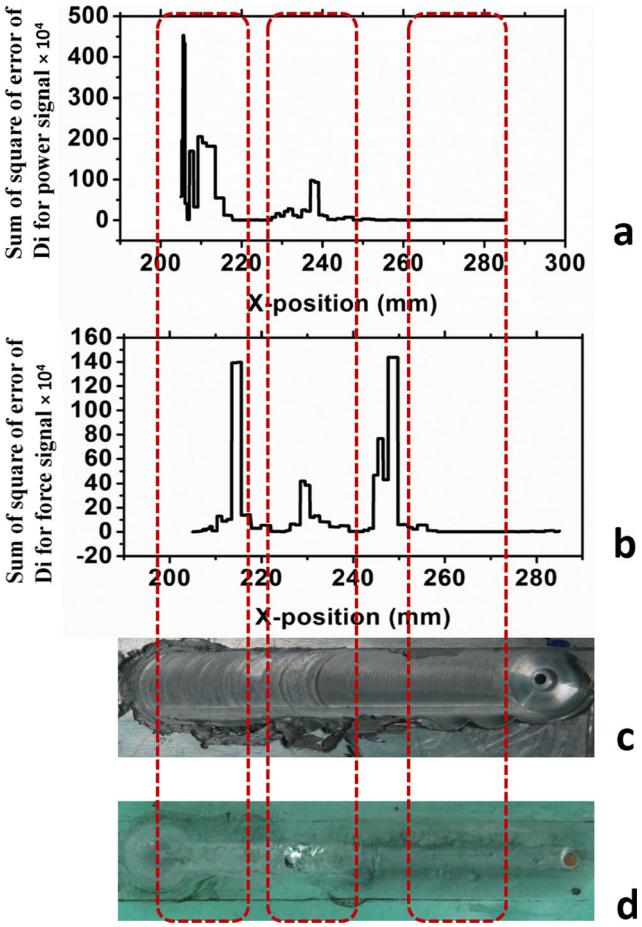

Fig. 16 **a** Plot of sum of square of errors of detailed coefficients (D_i) up to 5th level of decomposition of power signal versus X-position of the tool for sample 2. **b** Plot of sum of square of errors of detailed coefficients (D_i) up to 5th level of decomposition of force signal versus X-position of the tool for sample 2. **c** Front side of the welded sample 2. **d** Back side of the welded sample 2

The defects in the samples were measured by its length of occurrence. The fluctuations in the sum of square of errors were measured from the respective plots on MATLAB by its length of existence and then they were compared. To compare the extent of defect as obtained from the plot of sum of square of errors and that observed physically from the sample, coefficient of error matching (ρ_e) was defined as follows:

$\rho_{e1} = 1$, for the region where defect in sample is equal to the fluctuation in the plot of sum of square of errors.

$\rho_{e2} = -1$, for the region where there is a defect in the sample but not reflected in the plot of sum of square of errors.

$\rho_{e3} = = 0$, for the region where there is a fluctuation in the plot of sum of square of errors, but no defect in the sample.

The coefficent of error localization (χ_e) can be defined as :

$$\chi_e = \frac{(\rho_{e1}) \times x_1 + (\rho_{e2}) \times x_2 + (\rho_{e3}) \times x_3}{x_1 + x_2 + x_3} \tag{4}$$

x_1 is the length of region where there is defect in the sample as well as fluctuations are present in the plot of sum of square of errors. The corresponding coefficient of error matching is ρ_{e1}.

x_2 is the length of region where there is a defect in the sample but not reflected in the plot of sum of square of errors. The corresponding coefficient of error matching is ρ_{e2}.

x_3 is the length of region where there is a defect in the sample but no fluctuation in the plot of sum of square of errors. The corresponding coefficient of error matching is ρ_{e3}.

The value of χ_e can range from − 1 to + 1. It can be said that the level of decomposition showing the maximum value of χ_e , localizes the error best. Also, when the optimum level of decomposition is found out, comparison is made between force and power signal data as to which gives a greater value of χ_e . For a particular level of decomposition, if x_1 is more than x_2, then χ_e will be positive. The more x_1 dominates over x_2 the more the value of χ_e.

V. The CT scan images of the samples were studied for analyzing internal defects.

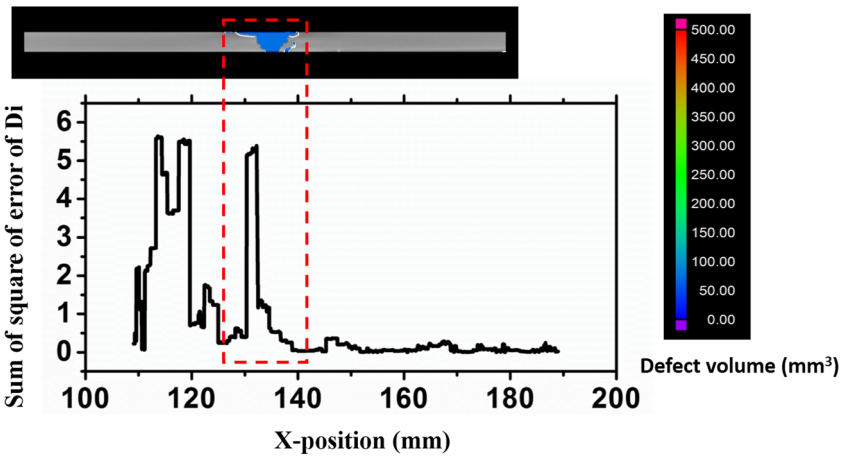

Fig. 17 Showing **a** CT scan image of the weld sample 1 showing internal defects and **b** plot of sum of square of errors of detailed coefficients (D_i) up to 5th level of decomposition of power signal versus X-position of the tool for sample 1

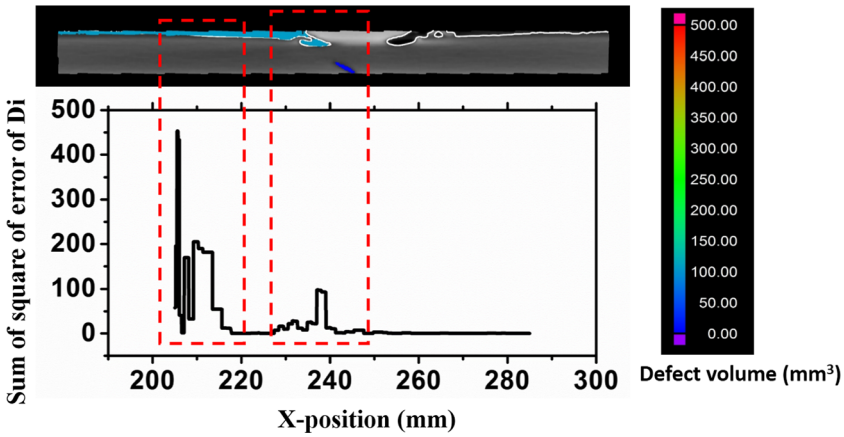

Fig. 18 Showing **a** CT scan image of the weld sample 2 showing internal defects and **b** Plot of sum of square of errors of detailed coefficients (D_i) up to 5th level of decomposition of power signal versus X-position of the tool for sample 2

3 Results and discussions

3.1 Experimental validation

Figures 3, 4, 5, 6 show the power and force versus time plots for both the samples. In both cases, median filter was applied in MATLAB.

When the FSW machine is turned on, all the components of it suddenly draw in huge current which results into initial peak in the power signal data.

From the time domain analysis of the signals, the time information (the starting and the ending time) of the welding was obtained. The corresponding X-position of the tool, i.e., the positions of the tool at each moment from the starting point of welding, was measured. From this power signal versus X-position of welding tool was plotted (Figs. 7 and 8). Similarly, it was done for the force signal (Figs. 9 and 10).

Negative values of force signal denote huge defect formation, as a result of which the tool fails to touch the weld sample.

In the power versus X-position, or force versus X-position plot of the weld zone, the abrupt change in the signal represents defect at that region.

It can be said that the sum of square of errors upto 5th level of decomposition gives the best result for both force and power signals (Table 2).

The nature of variation of χ_e corresponding to the proper detection of defects in the weld region has been discussed in Sect. 2.5. The decomposition was considered up to 6th level. Beyond that, the plot of sum of square of errors showed huge fluctuations throughout the working range. The machine vibration read by the sensors has a certain amplitude and frequency. These noises are not reflected for smaller levels of wavelet decompositions, but when the force and power data are decomposed beyond the 6th level six, the smaller fluctuations are also reflected in the plot of sum of square of errors. In those points, where fluctuations are present in the plot, physical defects may not be present.

Figures 11, 12, 13, and 14 show the variation of square of error of the detailed coefficients with the X-position of tool for power and force signals. Abrupt changes at some positions reflect presence of defects (Fig. 15).

Referring to Figs. 16 and 17, it is seen that fluctuations in sum of square of errors up to 5th level of decomposition of force and power signals correspond to defects occurring in the weld sample. Places where there is no such fluctuation in the plot represents smooth weld region.

3.1.1 CT scan

An X-ray computed tomography (CT) scan makes use of computer-processed combination of many X-ray images taken from different angles to produce total cross-sectional image of the object under scan. Here, in this study, weld samples were scanned for internal defect detection. The color code presented (Figs. 17, 18, 19, and 20) shows the volume of internal

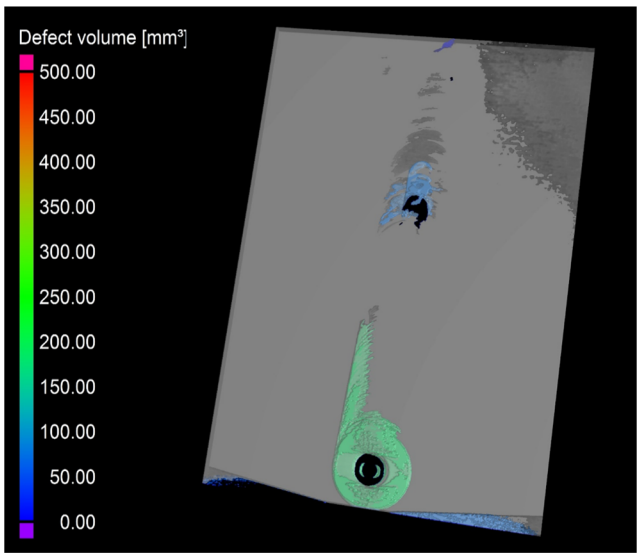

Fig. 19 CT scan image of the weld sample showing the surface and internal defects for sample 1

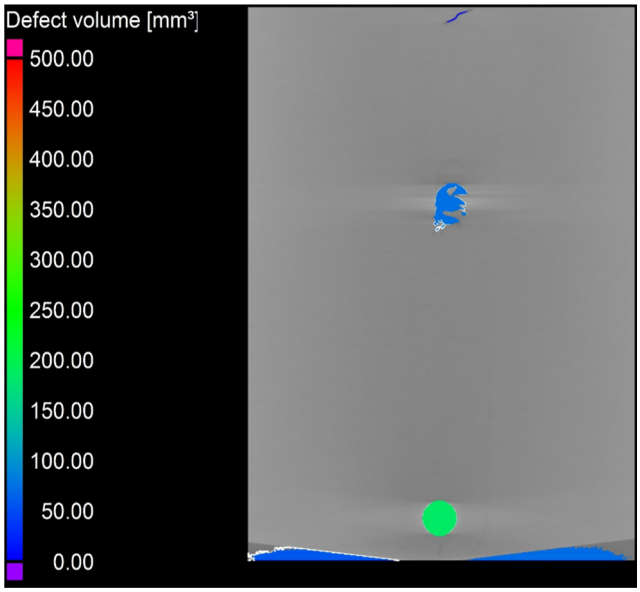

Fig. 20 CT scan image of the weld sample showing the surface defects for sample 2

defect(s). Only internal defects are colored and not the surface defects.

It may be noted that some additional peaks occur in the square of errors plot which do not correspond to internal or surface defects. These mainly occur due to unwanted noise and machine vibrations which add up to the force and power signal data.

In Fig. 19, the defect around the end of the weld region is due to heterogeneity of the sample and not due to the welding process.

4 Conclusion

DWT produces a time-frequency domain plot of the force signal and power signal data in FSW. Abrupt changes in the plots of detailed coefficients denote defects in the weld. It is found out that on implementing statistical tool, sum of square of errors, most accurate defect detection can be obtained by using 5th order wavelet decomposition. Some abrupt peaks in the plots reflect the defects mainly caused due to non-homogeneity of the material. One noticeable feature is that a few additional peaks occur in the sum of square of error plots which do not correspond to any surface defect. Most of these are due to internal defects within the weld. This has been verified from CT scan study of the materials. For analyzing defects, the power signal data has been found more effective than the force signal data. The force sensor is inbuilt in the FSW machine and hence some unwanted noise and vibrations of the machine add up to force signal data. However, the power sensor is connected by an external circuit to the machine and so the disturbances related to the machine do not add up to the power signal data. The power signal data represents the actual power consumed in the process. The results clearly localize both internal and surface defects in the weld by using 5th order DWT coefficients.

References

1. Walden S, Michael G, Temple-smith P (1995) 5:460–317
2. Citarella R, Carlone P, Lepore M, Palazzo GS (2015) Numerical-experimental crack growth analysis in AA2024-T3 FSWed butt joints. Adv Eng Softw 80:47–57. https://doi.org/10.1016/j.advengsoft.2014.09.018
3. Wang H, Colegrove PA, Mehnen J (2014) Hybrid modelling of the contact gap conductance heat transfer in welding process. Adv Eng Softw 68:19–24. https://doi.org/10.1016/j.advengsoft.2013.11.001
4. Benyounis KY, Olabi AG (2008) Optimization of different welding processes using statistical and numerical approaches - a reference guide. Adv Eng Softw 39:483–496. https://doi.org/10.1016/j.advengsoft.2007.03.012
5. Mandal S, Rice J, Elmustafa AA (2008) Experimental and numerical investigation of the plunge stage in friction stir welding. J Mater Process Technol 203:411–419. https://doi.org/10.1016/j.jmatprotec.2007.10.067
6. Kumar K, Kalyan C, Kailas SV, Srivatsan TS (2009) An investigation of friction during friction stir welding of metallic materials. Mater Manuf Process 24:438–445. https://doi.org/10.1080/10426910802714340
7. Cui S, Chen ZW, Robson JD (2010) A model relating tool torque and its associated power and specific energy to rotation and forward speeds during friction stir welding/processing. Int J Mach Tools Manuf 50:1023–1030. https://doi.org/10.1016/j.ijmachtools.2010.09.005
8. Kumar R, Singh K, Pandey S (2012) Process forces and heat input as function of process parameters in AA5083 friction stir welds. Trans Nonferrous Metals Soc China 22:288–298. https://doi.org/10.1016/S1003-6326(11)61173-4
9. Trimble D, Monaghan J, O'Donnell GE (2012) Force generation during friction stir welding of AA2024-T3. CIRP Ann Manuf Technol 61:9–12. https://doi.org/10.1016/j.cirp.2012.03.024
10. Pew JW, Nelson TW, Sorensen CD (2007) Torque based weld power model for friction stir welding. Sci Technol Weld Join 12:341–347. https://doi.org/10.1179/174329307X197601
11. Mehta M, Chatterjee K, De A (2013) Monitoring torque and traverse force in friction stir welding from input electrical signatures of driving motors. Sci Technol Weld Join 18:191–197. https://doi.org/10.1179/1362171812Y.0000000084
12. Su H, Wu CS, Pittner A, Rethmeier M (2013) Simultaneous measurement of tool torque, traverse force and axial force in friction stir welding. J Manuf Process 15:495–500. https://doi.org/10.1016/j.jmapro.2013.09.001
13. Razal Rose A, Manisekar K, Balasubramanian V (2011) Effect of axial force on microstructure and tensile properties of friction stir welded AZ61A magnesium alloy. Trans Nonferrous Metals Soc China 21:974–984. https://doi.org/10.1016/S1003-6326(11)60809-1
14. Chen C, Kovacevic R, Jandgric D (2003) Wavelet transform analysis of acoustic emission in monitoring friction stir welding of 6061

aluminum. Int J Mach Tools Manuf 43:1383–1390. https://doi.org/10.1016/S0890-6955(03)00130-5
15. Ramulu PJ, Narayanan RG, Kailas SV, Reddy J (2013) Internal defect and process parameter analysis during friction stir welding of Al 6061 sheets. Int J Adv Manuf Technol 65:1515–1528. https://doi.org/10.1007/s00170-012-4276-z
16. Fratini L, Buffa G (2005) CDRX modelling in friction stir welding of aluminium alloys. Int J Mach Tools Manuf 45:1188–1194. https://doi.org/10.1016/j.ijmachtools.2004.12.001
17. Jiménez-Macías E, Sánchez-Roca A, Carvajal-Fals H, Blanco-Fernández J, Martínez-Cámara E (2014) Wavelets application in prediction of friction stir welding parameters of alloy joints from vibroacoustic ANN-based model. Abstr Appl Anal 2014:1–11. https://doi.org/10.1155/2014/728564
18. Chen HB, Yan K, Lin T et al (2006) The investigation of typical welding defects for 5456 aluminum alloy friction stir welds. Mater Sci Eng A 433:64–69. https://doi.org/10.1016/j.msea.2006.06.056
19. Soundararajan V, Atharifar H, Kovacevic R (2006) Monitoring and processing the acoustic emission signals from the friction-stir-welding process. Proc Inst Mech Eng B J Eng Manuf 220:1673–1685. https://doi.org/10.1243/09544054JEM586
20. Bhat NN, Kumari K, Dutta S, Pal SK, Pal S (2015) Friction stir weld classification by applying wavelet analysis and support vector machine on weld surface images. J Manuf Process 20:274–281. https://doi.org/10.1016/j.jmapro.2015.07.002
21. Das B, Pal S, Bag S (2014) Monitoring of friction stir welding process through signals acquired during the welding. 1–7
22. Jose A, Babu AS, Kumar VSS (2013) Analysis of acoustic signals in friction stir welding. 161–164
23. Kumar U, Yadav I, Kumari S, Kumari K, Ranjan N, Kesharwani RK, Jain R, Kumar S, Pal S, Chakravarty D, Pal SK (2015) Defect identification in friction stir welding using discrete wavelet analysis. Adv Eng Softw 85:43–50. https://doi.org/10.1016/j.advengsoft.2015.02.001
24. Das B, Pal S, Bag S (2017) Weld quality prediction in friction stir welding using wavelet analysis. Int J Adv Manuf Technol 89:711–725. https://doi.org/10.1007/s00170-016-9140-0
25. Sinha P, Muthukumaran S, Sivakumar R, Mukherjee SK (2008) Condition monitoring of first mode of metal transfer in friction stir welding by image processing techniques. Int J Adv Manuf Technol 36:484–489. https://doi.org/10.1007/s00170-006-0854-2
26. Tansel IN, Demetgul M, Okuyucu H, Yapici A (2010) Optimizations of friction stir welding of aluminum alloy by using genetically optimized neural network. Int J Adv Manuf Technol 48:95–101. https://doi.org/10.1007/s00170-009-2266-6
27. Huggett DJ, Liao TW, Wahab MA, Okeil A (2017) Prediction of friction stir weld quality without and with signal features. Int J Adv Manuf Technol 95:1–15. https://doi.org/10.1007/s00170-017-1403-x
28. Babajanzade Roshan S, Behboodi Jooibari M, Teimouri R, Asgharzadeh-Ahmadi G, Falahati-Naghibi M, Sohrabpoor H (2013) Optimization of friction stir welding process of AA7075 aluminum alloy to achieve desirable mechanical properties using ANFIS models and simulated annealing algorithm. Int J Adv Manuf Technol 69:1803–1818. https://doi.org/10.1007/s00170-013-5131-6
29. Kamal Babu K, Panneerselvam K, Sathiya P, Noorul Haq A, Sundarrajan S, Mastanaiah P, Srinivasa Murthy CV (2017) Parameter optimization of friction stir welding of cryorolled AA2219 alloy using artificial neural network modeling with genetic algorithm. Int J Adv Manuf Technol 94:3117–3129. https://doi.org/10.1007/s00170-017-0897-6
30. Li JQ, Liu HJ (2014) Optimization of welding parameters for the reverse dual-rotation friction stir welding of a high-strength aluminum alloy 2219-T6. Int J Adv Manuf Technol 76:1469–1478. https://doi.org/10.1007/s00170-014-6352-z
31. Zhao S, Bi Q, Wang Y, Shi J (2017) Empirical modeling for the effects of welding factors on tensile properties of bobbin tool friction stir-welded 2219-T87 aluminum alloy. Int J Adv Manuf Technol 90:1105–1118. https://doi.org/10.1007/s00170-016-9450-2
32. Das B, Bag S, Pal S (2016) Defect detection in friction stir welding process through characterization of signals by fractal dimension. Manuf Lett 7:6–10. https://doi.org/10.1016/j.mfglet.2015.11.006
33. Adelson EH, Anderson CH, Bergen JR, Burt PJ, Ogden JM (1984) Pyramid methods in image processing. RCA Eng:33–41
34. Ranjan R, Reza A, Parikh C et al (2016) Classification and identification of surface defects in friction stir welding: an image processing approach. J Manuf Process 22:237–253. https://doi.org/10.1016/j.jmapro.2016.03.009
35. Kumari S, Jain R, Kumar U, Yadav I, Ranjan N, Kumari K, Kesharwani RK, Kumar S, Pal S, Pal SK, Chakravarty D (2016) Defect identification in friction stir welding using continuous wavelet transform. J Intell Manuf 1–12. https://doi.org/10.1007/s10845-016-1259-1
36. Das B, Pal S, Bag S (2016) A combined wavelet packet and Hilbert-Huang transform for defect detection and modelling of weld strength in friction stir welding process. J Manuf Process 22:260–268. https://doi.org/10.1016/j.jmapro.2016.04.002
37. Parikh C, Ranjan R, Khan AR, Jain R, Mahto RP, Chakravarty D, Pal S, Pal SK (2017) Volumetric defect analysis in friction stir welding based on three dimensional reconstructed images. J Manuf Process 29:96–112. https://doi.org/10.1016/j.jmapro.2017.07.006
38. Sahu PK, Kumari K, Pal S, Pal SK (2016) Hybrid fuzzy-grey-Taguchi based multi weld quality optimization of Al/cu dissimilar friction stir welded joints. Adv Manuf 4:237–247. https://doi.org/10.1007/s40436-016-0151-8
39. Liu F, Liu S, Guo E, Li L (2008) Ultrasonic evaluation of friction stir welding. 17th World Conf Nondestruct. 25–28